BOR DERGİSİ
JOURNAL OF BORON
https://dergipark.org.tr/boron

Effect of Fe doping on photocatalytic activity of B_2O_3 processed using polyvinyl borate precursor

Özcan Köysüren*

Ankara University, Department of Energy Engineering, Ankara, 06830, Turkey, ORCID ID orcid.org/0000-0002-5578-1145

ARTICLE INFO

Article history:
Received 24 July 2019
Received in revised form 03 November 2019
Accepted 17 December 2019
Available online 31 December 2019

Research Article

DOI: 10.30728/boron.596150

Keywords:
B_2O_3,
Fe doping,
Photocatalytic activity,
Polyvinyl borate,
UV light irradiation.

ABSTRACT

In this study, boron oxide (B_2O_3) powder has been synthesized by the pyrolysis of polyvinyl borate precursor in air. For this purpose, polyvinyl borate precursor was synthesized through the condensation reaction of polyvinyl alcohol and boric acid, and then the polymeric precursor was pyrolyzed at 500°C. The as-prepared B_2O_3 particles were doped with iron (Fe) ions using the wet impregnation method. The photocatalytic activity of both undoped B_2O_3 and iron doped B_2O_3 (Fe-B_2O_3) powders was studied by investigating the degradation of the model dye, methylene blue, under UV light irradiation. It was pointed out that iron doped B_2O_3 powder exhibited enhanced photocatalytic activity compared to undoped one. In addition, various techniques of characterization such as FTIR, XRD, FESEM, EDX and UV–Vis spectroscopy were performed to confirm the synthesis of B_2O_3 particles and the presence of iron ions in the crystal structure of the prepared photocatalyst. The novelty of this study was to research the photocatalytic performance of both B_2O_3 and Fe-B_2O_3 photocatalysts.

1. Introduction

Currently, there has been great demand for boron and boron-related compounds such as B_2O_3, boron carbide (B_4C) and boron nitride (BN) owing to their unique properties such as high temperature stability, chemical stability, hardness and wear resistance [1]. B_2O_3 is a common component for large-scale industrial applications such as flame retardants, fiberglass and optical glasses. B_2O_3 particles are also utilized in radiation shielding and dielectric applications [2]. B_2O_3 can be used as additives to improve textural and acid-base properties of common metal oxides [3]. B_2O_3 can also be utilized in the industry as a raw component for the processing of commercial alloys and it can be used as a precursor for the synthesis of common compounds like TiB_2 and MoB_2 [4]. In addition, the capability of B_2O_3 for thermochemical energy storage has been studied. Although thermochemical energy storage systems are still at an experimental stage, they are important because they have the potential to store energy from renewable energy and waste heat sources [5].

Few studies on synthesis of B_2O_3 powder are available in the literature. B_2O_3 can be processed in bulk form through sintering at high temperatures using specialized equipment. Apart from the bulk shape, B_2O_3 can be processed in nanopowder form using ball milling, chemical vapor deposition or sonochemical techniques. Although the ball milling method is inexpensive and simple, it exhibits limitations with respect to the homogeneity of products synthesized. The sonochemical technique requires special, expensive and toxic chemicals like the capping agent in the production of nanopowder B_2O_3 [2]. On the other hand, B_2O_3 nanoparticles can be processed under vacuum at high temperatures through the chemical vapor deposition technique [1].

Apart from the specified techniques, B_2O_3 powder can be synthesized using polyvinyl borate precursor through relatively low-temperature exothermic reactions [6-8]. The heat treatment of polyvinyl borate precursor provides the formation of B_2O_3 powder, composed of submicron size particles. There are some advantages of the specified technique such as being relatively simple and inexpensive to process B_2O_3 powder in large quantities. Polyvinyl borate-like precursors, synthesized from nonhazardous and inexpensive reactants, have received attention in the synthesis of B_2O_3 powder through a relatively low-temperature process. In addition to B_2O_3, boron carbide structures can also be obtained by the heat treatment of the polymer precursor [7,8]. In order to increase the B_2O_3 content of the heat treatment product, the reaction mechanisms need to be fully understood. It is known that B_2O_3 synthesis reactions are governed by heterogeneous oxidation. The transport of the reactants through the oxide layer of B_2O_3 may limit the oxidation reaction [6]. It is not easy to control both

*Corresponding author: koysuren@ankara.edu.tr

the B_2O_3 content and the morphology of the product powder. By changing the boron content of the precursor and the pyrolysis temperature, it has been tried to change the crystal structure and B_2O_3 content in the powder product [7,8].

Photocatalysis is known as a green method, especially for a series of environmental applications like the removal of organic dyes from the wastewater. In this method, semiconducting photocatalysts, such as TiO_2, ZnO, SnO_2 and $SrTiO_3$, can produce reactive and oxidizing free radicals from the oxygen and the water by means of UV light, which succeed in a high degradation for organic dye pollutants [9,10]. The specified photocatalysts have many advantages such as high photocatalytic activity, stability in aqueous medium, low cost and reusability. The semiconducting photocatalysts can produce photoinduced charge carriers, electron-hole pair, and the following powerful superoxide and hydroxyl radicals to provide the photocatalytic degradation of organic dye molecules under UV light irradiation [10,11].

There is a major drawback to the use of the semiconductors as photocatalyst for the degradation of organic dye molecules in the treatment of wastewater. The recombination of the photoexcited electron-hole pairs reduces the photocatalytic degradation efficiency [9]. To suppress the specified drawback, various approaches like metal ion doping have been reported to enhance the photocatalytic efficiency by reducing the recombination rate of photoexcited electron-hole pairs [9, 10]. Photoinduced electrons in the conduction band and photoinduced holes in the valence band possess high reduction power and oxidation power, respectively. The presence and the amount of the photoexcited charge carriers are significant prerequisites to realize the photocatalysis successfully [9]. In literature, metal ions possessing similar properties to elements of the photocatalyst have been studied since they are able to substitute elements in the photocatalyst during the doping process [10]. Among various metal ions such as Ag, Au, B, Zn, Ni, Ce, Cr and Al, Fe has been considered as an effective candidate for the doping of the semiconducting photocatalysts like TiO_2 [12], Ag_2S [13], CeO_2 [14], ZnO [15] and C_3N_4 [16]. Fe doping might accelerate the separation of the photoinduced charge carriers, which gave rise to an increase in formation of the oxidizing free radicals. Hence, Fe doped photocatalysts exerted enhanced photocatalytic performance in the degradation of organic pollutants under UV light irradiation.

In literature, there is no study on the photocatalytic performance of pure B_2O_3 due to its low catalytic efficiency. On the other hand, B_2O_3 was combined with TiO_2 [17], Bi_2O_3 [18], ZrO_2 [19] and SiO_2 [20] in composite structure. With B_2O_3 contribution, the optical band gap of the photocatalyst systems changed and the light absorption spectrum of the composite photocatalysts exhibited a red shift. In general, the photocatalytic activity of the photocatalyst systems enhanced by the content of B_2O_3. In the scope of this study, B_2O_3 powder was synthesized by employing a relatively simple, inexpensive and low-temperature synthesis using polyvinyl borate precursor. Given the above consideration, the photocatalytic performance of pure B_2O_3 was studied for the first time by evaluating the degradation of methylene blue under UV light irradiation. Additionally, Fe doping was applied to B_2O_3 particles for the first time to enhance its photocatalytic activity.

2. Materials and methods

2.1. Preparation of B_2O_3 and Fe-B_2O_3 photocatalysts

Polyvinyl alcohol (PVA) (molecular weight 89000-98000 g/mol and 99 mol.% hydrolyzed), boric acid (H_3BO_3), methylene blue and iron nitrate nonahydrate ($Fe(NO_3)_3•9H_2O$) were obtained from Sigma-Aldrich. All chemicals were used without further purification. Polyvinyl borate (PVB) precursor was synthesized via the condensation reaction of PVA and H_3BO_3 in a B–OH: PVA–OH molar ratio of 1.4:1. PVA (2.0 g) was dissolved in 50 ml of distilled hot water (80°C) with constant stirring. At the same time, H_3BO_3 (2.0 g) was dissolved in 50 ml of distilled water by stirring. Then, the boric acid solution was added to the PVA solution with constant stirring for half an hour, which gave rise to PVB precursor in gel form. Afterwards, PVB precursor after drying at 120°C was ground to powder. PVB precursor powders were placed in a porcelain crucible and pyrolyzed in a furnace at 500°C for 3 hours to obtain B_2O_3 powders [7,8].

In accordance with the literature, the wet impregnation method was used for the preparation Fe doped B_2O_3 (Fe-B_2O_3) [20]. In detail, appropriate amount of $Fe(NO_3)_3•9H_2O$ was dissolved in 100 ml of distilled water followed by addition of 2 g of B_2O_3 powder into the as-prepared solution under constant stirring for about 3 hours. Then, the resultant slurry was filtered off, washed with distilled water and dried at 100 °C for about 24 hours. Eventually, the obtained substance was ground and calcined at 500°C for 3 hours. Fe ion content of B_2O_3 was chosen as 2 wt.% [21].

2.2. Methods of characterization

Fourier transform infrared (FTIR) spectroscopy was monitored by a IFS 66/S (Bruker) spectrophotometer to investigate the bonding structure of B_2O_3 and Fe-B_2O_3 powders. XRD patterns of the prepared samples were recorded using a Rigaku Ultima IV diffractometer (Cu Kα source, λ = 1.54 Å) over a 2Θ range from 10° to 50°. UV–Vis absorption spectra were obtained by a Thermo Scientific (Genesys 10S) UV-Vis spectrophotometer to analyze the optical properties of B_2O_3 and

Fe-B_2O_3 powders. A field emission scanning electron microscope (FESEM) (QUANTA 400F) equipped with EDX (Energy dispersive X-ray) Microanalysis Instrument (JXA-8230) was used to obtain the micrographs of the prepared samples.

The photocatalytic activity of B_2O_3 and Fe doped B_2O_3 powders was researched by the degradation of methylene blue as a model reaction. In a typical analysis, B_2O_3 powder and Fe-B_2O_3 powder (1 g/l), separately, were dispersed into the dye (methylene blue) solution (10 mg/l). The test medium was held in the dark for 30 minutes for an adsorption-desorption equilibrium between B_2O_3 and the dye molecules. Then, the dye solution was exposed to UV light (30 W, UVC) irradiation. The distance between the UV light source and the reaction medium was 15 cm. The degradation of methylene blue, monitored by the Thermo Scientific (Genesys 10S) UV-Vis spectrophotometer, was taken as a model reaction to analyze the photocatalytic performance of B_2O_3 and Fe-B_2O_3, respectively. After a fixed irradiation time period, samples of methylene blue solution (3 ml) were withdrawn from the test medium and the quantitative determination of methylene blue was performed by measuring its absorption at 665 nm with the UV–Vis spectrophotometer. Percentage degradation of the model dye was calculated by using the following relation [18]:

$$\text{Percent degradation (\%)} = [(C_0 - C_t) / C_0] \times 100 \quad (1)$$

where C_0 and C_t are the concentration of methylene blue initially and after UV light irradiation, respectively.

3. Results and discussion

3.1. FTIR analysis

FTIR spectrum of B_2O_3 powder and Fe-B_2O_3 powder are shown in Figure 1. FTIR spectrum of undoped B_2O_3 shows a broad transmission band at around 3219 cm^{-1} (Figure 1a), which was attributed to O-H vibration due to the presence of surface adsorbed water molecules or hydroxyl ions of PVB precursor [8,22]. The weak transmission peak at 2968 cm^{-1} was assigned to C-H stretching vibration of PVB precursor, which indicates that almost all of the PVB chains were degraded during the pyrolysis [8,23]. Broad transmission bands between 1600-1250 cm^{-1} with a peak at 1421 cm^{-1} and between 1000-500 cm^{-1} were related to B-O stretching vibration, which suggested the formation of B_2O_3 nanoclusters [8,23]. The transmission peak at 1143 cm^{-1} was assigned to B-C stretching vibration (Figure 1a), confirming the formation of boron carbide (B_4C) structures together with B_2O_3 clusters [7,8]. In general, the spectrum of Fe doped B_2O_3 resembles to that of the undoped one (Figure 1b). FTIR spectrum of Fe-B_2O_3 also consists of two broad transmission bands at around 1432 cm^{-1} and between 1000-400 cm^{-1}, corresponding to B-O stretching vibration of B_2O_3 structure [8,23]. Some stronger vibration for Fe doped B_2O_3 between 1000-400 cm^{-1} might be due to metal vibration in this region, which confirmed the presence of Fe ions within B_2O_3 structure [22]. In addition, transmission peaks observed at 3216 cm^{-1}, 2958 cm^{-1} and 1182 cm^{-1} were related to O-H, C-H and B-C bonds, respectively [7,8,23]. Also, the weak transmission peak at 1604 cm^{-1} was related to C-N stretching vibration. C-N structure might occur during the doping process of B_2O_3 with $Fe(NO_3)_3 \cdot 9H_2O$ [24].

3.2. XRD analysis

Figure 2 exhibits XRD spectra of undoped B_2O_3 and Fe-B_2O_3 powders. The diffraction peaks seen at the angles 14.06°, 27.94° and 39.64° were in agreement with the cubic crystalline B_2O_3 structure (Figure 2a). The two peaks at the angles 27.94° and 39.64° were related to (310) and (420) crystal planes of the cubic B_2O_3 structure, respectively [3]. The broad diffraction peak centered at about 25.6° was attributed to

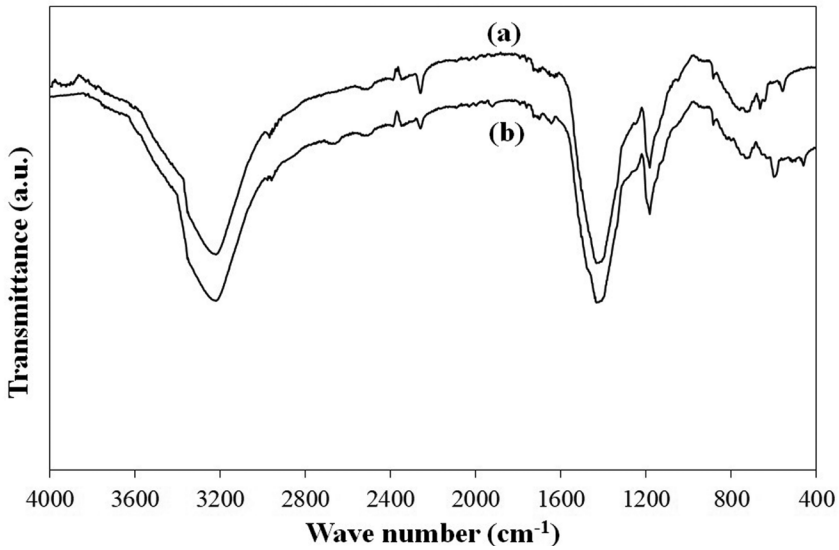

Figure 1. FTIR spectra of (a) B_2O_3 and (b) Fe-B_2O_3.

amorphous carbon phase, which might arise from the PVB precursor [3]. The diffraction peaks of Fe-B_2O_3 appear almost at the same positions with only slight changes in position and intensity of the peaks due to Fe doping (Figure 2b). The diffraction peaks observed at the angles 14.38°, 27.82° and 39.70° agree with the cubic crystalline structure of B_2O_3. No additional peaks were observed on the XRD spectrum of Fe-B_2O_3. One of the possible reasons might be the formation of the solid solution by substituting B^{3+} or O^{-2} ions with Fe ions in the B_2O_3 lattice. Another possible reason might be the presence of finely dispersed iron oxides on the B_2O_3 surface [14]. XRD results proved that the pyrolysis of PVB precursor gave rise to B_2O_3 crystalline structure with amorphous carbon phase and Fe doping did not result any change in the cubic crystalline structure of B_2O_3 due to the low quantity of the dopant atom.

3.3. Morphological analyses

Many models have been proposed to identify the reaction mechanism of the B_2O_3 synthesis. Specifically, it was proposed that the transport of the reactants, oxygen and boron, through the oxide layer limits the rate of the synthesis reaction. The specified model is based on the assumption that B_2O_3 particles are in regular spherical shape. However, similar to many studies in the literature, real B_2O_3 particles have a complex morphology [6] (Figure 3). B_2O_3 powder was composed of irregular shaped particles with sizes in the range from 100 to 1000 nm and the incorporation of Fe ions did not change the irregular shape and the average size of the B_2O_3 particles. Hence, the proposed model failed in describing the reaction mechanism of the B_2O_3 synthesis [6]. SEM images of both samples show crystal layers on amorphous phase, which means that the precursor could not be completely converted to the B_2O_3 crystal phase (Figure 3). It was also observed by XRD and EDX analyses. XRD patterns of both samples illustrate diffraction peaks belonging to the amorphous carbon structure. EDX analysis was performed to check on the elemental composition of both samples. EDX spectra revealed the presence of the B, O, and C elements on B_2O_3 and Fe-B_2O_3 particles (Figure 3). Additionally, the Fe element was observed on EDX spectrum of Fe-B2O3, which proved the presence of Fe ions within the B_2O_3 structure. Fe/B_2O_3 weight ratio (1.86), obtained by EDX analysis, was comparable to the experimental ratio (Table 1).

3.4. Optical property

The optical properties of the photocatalyst powders were examined by UV–Vis absorption spectroscopy. Figure 4 illustrates the comparative UV–Vis absorption spectra of B_2O_3 and Fe-B_2O_3. Both B_2O_3 and Fe-B_2O_3 powders exhibited high absorbance over the entire UV light and visible light regions of the electromagnetic spectrum. The optical band gap energy of the prepared samples was estimated using the Tauc plot, obtained from the absorbance as a function of the wavelength of the incident light. In order to calculate the optical band gap energy of B_2O_3 and Fe-B_2O_3 samples, $(\alpha h\nu)^2$ vs. the photon energy (hv) was plotted and then the linear part of the drawn curve was extrapolated to x-axis (Figure 5), which gave an estimate of the optical band gap energy of B_2O_3 and Fe-B_2O_3 samples [18]. Based on the Tauc plot analysis (Figure 5), the corresponding optical band gap energies were estimated to be 1.5 eV and 2.4 eV for B_2O_3 and Fe-B_2O_3, respectively. The increase in the optical band gap energy could

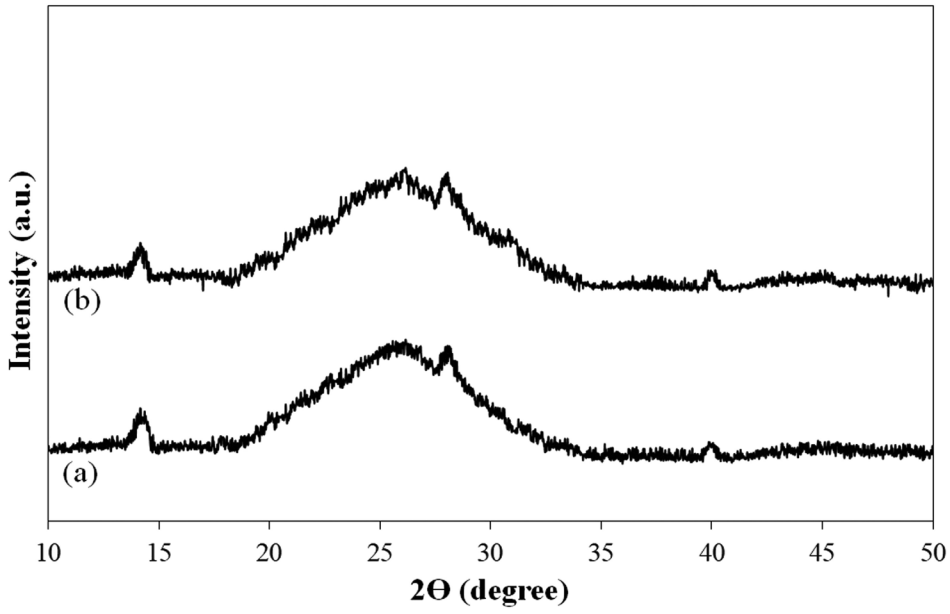

Figure 2. XRD patterns of (a) B_2O_3 and (b) Fe-B_2O_3.

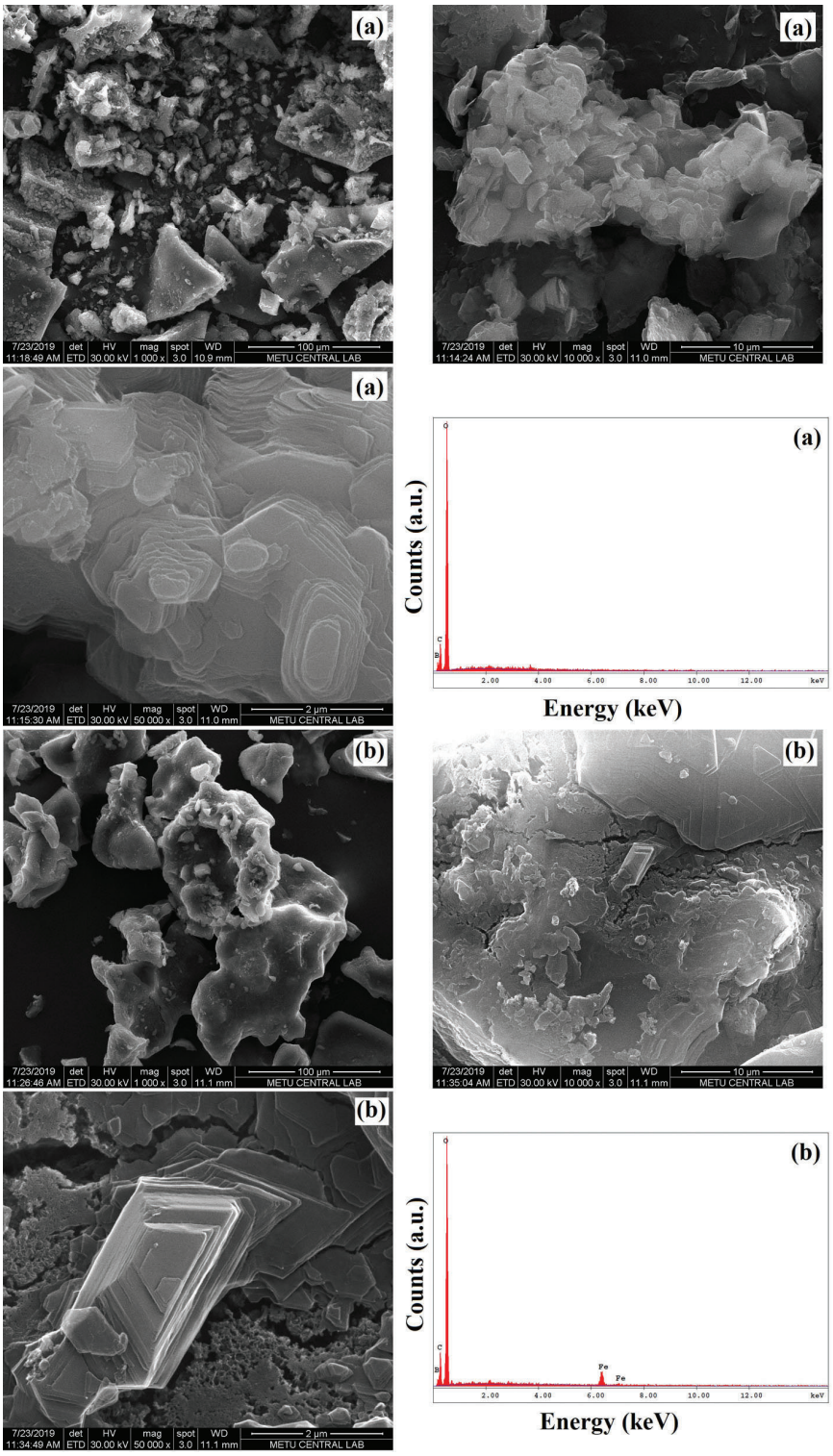

Figure 3. FESEM images and EDX spectra of (a) B_2O_3 and (b) Fe-B_2O_3.

Table 1. The percentage of constituent elements in B_2O_3 and Fe-B_2O_3, respectively.

Sample	Boron (wt.%)	Oxygen (wt.%)	Carbon (wt.%)	Iron (wt.%)
B_2O_3	30.64	45.73	23.64	-
Fe-B_2O_3	27.81	44.60	26.24	1.35

be related to the following increase in charge carrier concentration, which hindered the lower energy states of the conduction band in B_2O_3. This phenomenon is known as the Burstein–Moss effect [25]. According to the literature, the mentioned increase in the band gap energy of B_2O_3 upon Fe doping could be corresponded to the quantization size effect, monitored as the B_2O_3 particle size moves toward the Bohr radius value [26]. This assumption did not seem very likely since the average particle size of both B_2O_3 and Fe-B_2O_3 were quite larger than the Bohr radius value.

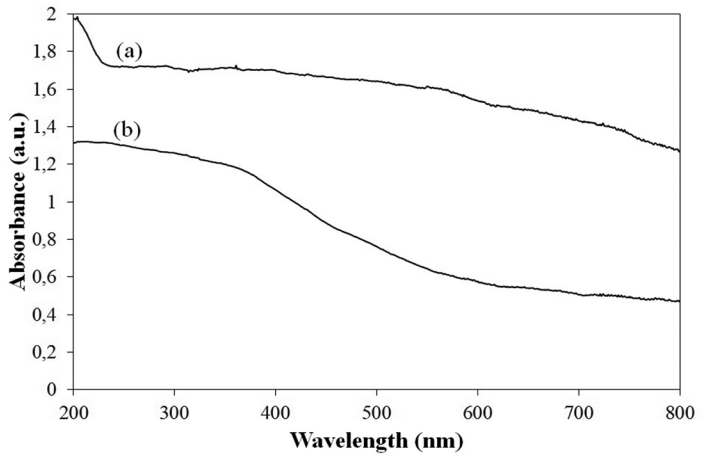

Figure 4. UV-Vis spectra of (a) B_2O_3 and (b) Fe-B_2O_3.

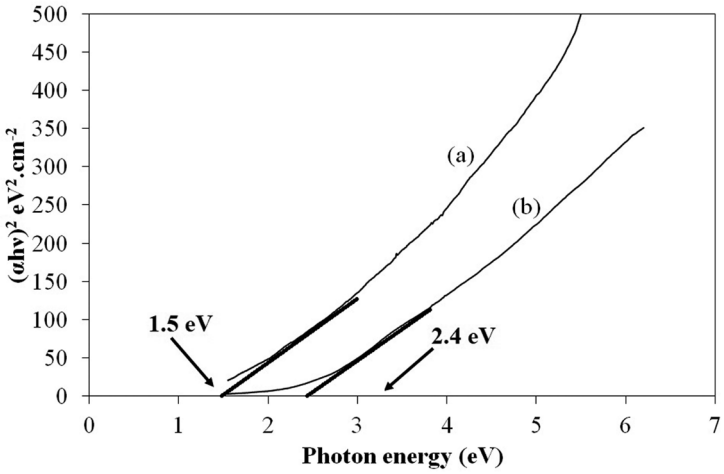

Figure 5. Tauc plots of (a) B_2O_3 and (b) Fe-B_2O_3.

3.5. Photocatalytic activity

UV-Vis absorption spectral variations during the photocatalytic degradation of methylene blue with B_2O_3 and Fe-B_2O_3 powders, separately, are shown in Figure 6. B_2O_3 powder doped with Fe ions was more photoactive in the process of methylene blue degradation in comparison to undoped B_2O_3 (Figure 7). The photocatalytic activity of B_2O_3 improved slightly by incorporating Fe ions into B_2O_3 structure, which might be due the substitution of boron or oxygen ions by Fe ions in B_2O_3 crystal lattice [17]. Fe ion radius is similar to B_3^+ and O^{2-} ions in size. During the calcination process, Fe ions might penetrate into B_2O_3 structure and could easily be replaced by boron or oxygen ions [17,27]. B_2O_3 and Fe-B_2O_3 achieved almost 12% and 20% dye degradation, respectively, after 150 minutes (Figure 7). The higher photocatalytic activity might indicate a more effective interfacial electron transfer between the conduction band of B_2O_3 and that of Fe ion, which provided better charge separation and therefore less recombination of photoinduced electrons with holes [27].

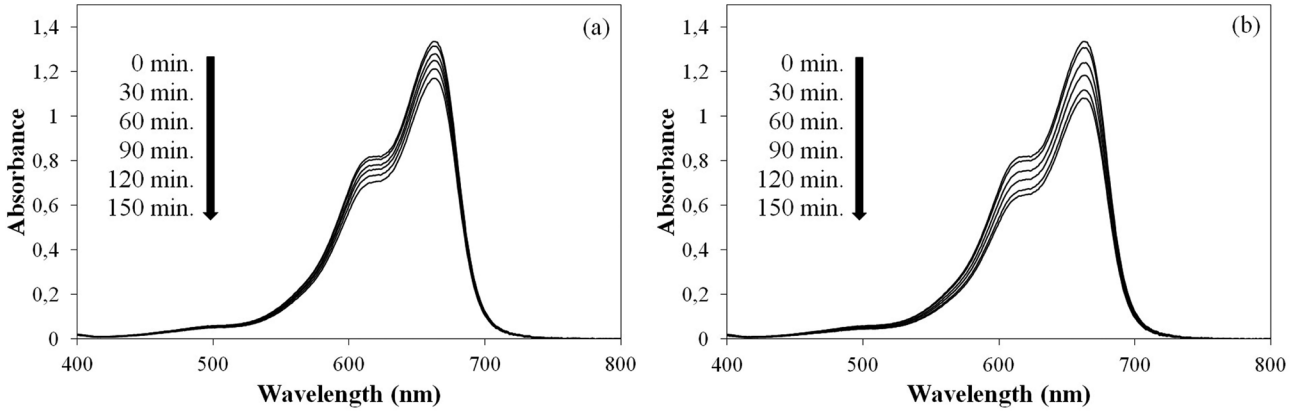

Figure 6. UV–Vis spectra of methylene blue solution in the presence of (a) B_2O_3 and (b) Fe-B_2O_3.

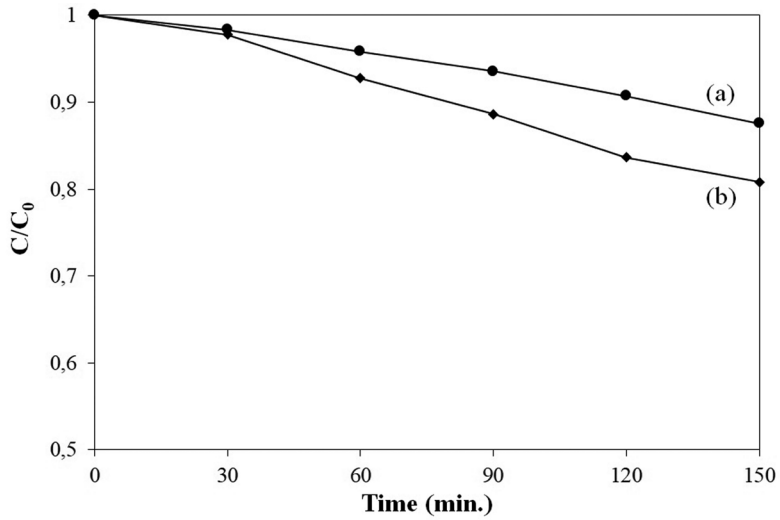

Figure 7. The relative concentration (C/C_0) of methylene blue vs. irradiation time for (a) B_2O_3 and (b) Fe-B_2O_3.

The rate of photocatalytic degradation was estimated by fitting the experimental data to the the pseudo-first order kinetic model [28]:

$$\ln(C_0/C_t) = kt \qquad (2)$$

where C_0 and C_t are methylene blue concentrations at times t = 0 and t = t, respectively and *k* is the apparent rate constant obtained by plotting $\ln (C_0/C_t)$ against the irradiation time (t). The fairly good correlation between $\ln (C_0/C_t)$ and t in both cases gave rise to high R^2 values close to 1 (Figure 8), which confirmed that the photocatalytic degradation of methylene blue could be described by the pseudo first-order kinetic model [27,28]. The apparent rate constant of undoped B_2O_3 was 0.0008 min^{-1}. After incorporation of Fe ions into the B_2O_3 structure, the photocatalytic activity potential of B_2O_3 was greatly enhanced. Its rate constant value was 0.0014 min^{-1}. The degradation rate of methylene blue for Fe-B_2O_3 was almost 1.75 times faster.

In accordance with the literature, a plausible mechanism was proposed to describe the photocatalytic degradation of methylene blue under UV light irradiation. Upon exposure of UV light, electrons in the valence band of B_2O_3 might excite to the conduction band of the photocatalyst, which provided the formation of the photoexcited electron-hole pair. Then, the photoexcited holes might react with water molecules to form hydroxyl radicals and the photoinduced electrons might interact with oxygen molecules to generate superoxide radicals. The highly active radicals could provide the degradation of the methylene blue molecules into H_2O and CO_2. Fe ions of Fe-B_2O_3 might form transfer channels for the photoinduced electron-hole pair, suppressing the recombination of the specified charge carriers [27,29]. Hence, the doping mechanism significantly increased the photocatalytic efficiency of B_2O_3.

4. Conclusions

In the present study, B_2O_3 powder was synthesized by the pyrolysis of polyvinyl borate precursor and the as-prepared B_2O_3 was doped by being substituted with Fe ions. FTİR, XRD, SEM, EDX and UV-Vis spectroscopy revealed the formation of B_2O_3 structure and the

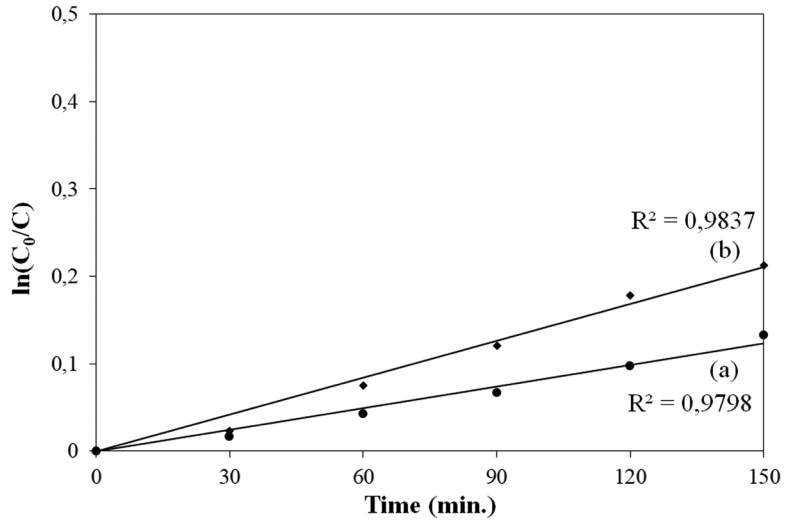

Figure 8. Photocatalytic degradation kinetics of methylene blue in the presence of (a) B_2O_3 and (b) Fe-B_2O_3

presence of Fe species within the B_2O_3 lattice. Doping of B_2O_3 with Fe species did not alter the morphology and the crystal structure of the photocatalyst much. When compared with undoped B_2O_3, the photocatalyst modified with Fe ions showed a higher photocatalytic activity in methylene blue degradation, which might be due to the incorporation of Fe ions into the lattice of B_2O_3.

References

[1] Alizadeh M., Sharifianjazi F., Haghshenasjazi E., Aghakhani M., Rajabi L., Production of nanosized boron oxide powder by high-energy ball milling, Synth. React. Inorg. Met.-Org. Nano-Metal Chem., 45 (1), 11-14, 2015.

[2] Ramachandran R., Jung D., Bernier N. A., Logan J. K., Waddington M. A., Spokoyny A. M., Sonochemical synthesis of small boron oxide nanoparticles, Inorg. Chem., 57, 8037−8041, 2018.

[3] Yang Q., Sha J., Wang L., Zou Y., Niu J., Cui C., Yang D., Crystalline boron oxide nanowires on silicon substrate, Physica E, 27, 319–324, 2005.

[4] Bhomia J., Sharma J., Sharma R. A., Singh Y., Some boron compounds of semicarbazones: Antimicrobial activity and precursor for the sol–gel transformation to nanosized boron oxide, New J. Chem., 42, 10376-10385, 2018.

[5] Huber C., Jahromy S. S., Jordan C., Schreiner M., Harasek M., Werner A., Winter F., Boric acid: A high potential candidate for thermochemical energy storage, Energies, 12 (6), 1086 (1-17), 2019.

[6] Sun Y., Chintersingh K. L., Schoenitz M., Dreizin, E. L., Reactive shell model for boron oxidation, J. Phys. Chem. C, 123 (18), 11807-11813, 2019.

[7] Yanase I., Ogaware R., Kobayashi H., Synthesis of boron carbide powder from polyvinyl borate precursor, Mat. Let., 63, 91-93, 2009.

[8] Mondal S., Banthia A. K., Low-temperature synthetic route for boron carbide, J Europ. Ceramic Soc., 25 (2-3), 287-291, 2005.

[9] Nanaji K., Janardhana R. K. S. K., Rao T. N., Anandan S., Energy level matching for efficient charge transfer in Ag doped - Ag modified TiO_2 for enhanced visible light photocatalytic activity, J. Alloys Compd., 794, 662-671, 2019.

[10] Wang X., Wang X. J., Song J. K., Li Y., Wang Z. C., Gao Y. X., A highly efficient TiO_X (X = N and P) photocatalyst for inactivation of Microcystis aeruginosa under visible light irradiation, Sep. Purif. Technol., 222, 99-108, 2019.

[11] Wang X., Feng, X., Shang J., Efficient photoelectrochemical oxidation of rhodamine B on metal electrodes without photo catalyst or supporting electrolyte, Front. Environ. Sci. Eng., 12 (6), 1-6, 2018.

[12] Li G., Wang B. D., Sun Q., Xu W. Q., Han Y. F., Visible-light photocatalytic activity of Fe and/or Ni doped ilmenite derived-titanium dioxide nanoparticles, J. Nanosci. Nanotechnol., 19 (6), 3343-3355, 2019.

[13] Ding Y., Liu H., Gao L. N., Fu M., Luo X., Zhang X., Liu Q., Zeng R. C., Fe-doped Ag_2S with excellent peroxidase-like activity for colorimetric determination of H_2O_2, J. Alloys Compd., 785, 1189-1197, 2019.

[14] Wen W., Lou Z., Chen Y., Chen D., Tian S., Xiong Y., Tuning the structural properties of CeO_2 by Pr and Fe codoping for enhanced visible-light catalytic activity, J. Chem. Technol. Biotechnol., 94 (5), 1576-1584, 2019.

[15] Chai H. Y., Lam S. M., Sin J. C., Green synthesis of magnetic Fe-doped ZnO nanoparticles via Hibiscus rosa-sinensis leaf extracts for boosted photocatalytic, antibacterial and antifungal activities, Mater. Lett., 242, 103-106, 2019.

[16] Xu Y., Ge F., Chen Z., Huang S., Wei W., Xie M., Xu H., Li H., One-step synthesis of Fe-doped surface-alkalinized g-C_3N_4 and their improved visible-light photocatalytic performance, Appl. Surf. Sci., 469, 739-746, 2019.

[17] Jung K. Y., Park S. B., Ihm S. K., Local structure and photocatalytic activity of B_2O_3-SiO_2/TiO_2 ternary mixed oxides prepared by sol-gel method, Appl. Catal., B, 51 (4), 239-245, 2004.

[18] Sharma S. K., Singh V. P., Chauhan V. S., Kushwaha H. S., Vaish R., Photocatalytic self-cleaning transparent 2Bi(2)O(3)-B_2O_3 glass ceramics, J. Appl. Phys., 122 (9), 094901 (1-12), 2017.

[19] Zhu L. Y., Wang X. Q., Zhang G. H., Ren Q., Xu D., Structural characterization and photocatalytic activity of B_2O_3/ZrO_2-TiO_2 mesoporous fibers, Appl. Catal., B, 103 (3–4), 428-435, 2011.

[20] Resende S. F., Gouveia R. L., Oliveira B. S., Vasconcelos W. L., Augusti R., Synthesis of TiO_2/SiO_2-B_2O_3 Ternary Nanocomposites: Influence of Interfacial Properties on their Photocatalytic Activities with High Resolution Mass Spectrometry Monitoring, J. Braz. Chem. Soc., 28 (10), 1995-2003, 2017.

[21] Jinisha R., Gandhimathi R., Ramesh S. T., Nidheesh P. V., Velmathi S., Removal of rhodamine B dye from aqueous solution by electro-Fenton process using iron-doped mesoporous silica as a heterogeneous catalyst, Chemosphere, 200, 446-454, 2018.

[22] Pirinejad L., Maleki A., Shahmoradi B., Daraei H., Yang J. K., Lee S. M., Synthesis and application of Fe-N-Cr-TiO_2 nanocatalyst for photocatalytic degradation of Acid Black 1 under LED light irradiation, J. Mol. Liq., 279, 232-240, 2019.

[23] Barros P. M., Yoshida V. P., Schiavon M. A., Boron-containing poly(vinyl alcohol) as a ceramic precursor, J. Non-Cryst. Solids, 352, 3444–3450, 2006.

[24] Mu Z., Hua J., Kumar H. S., Yang T. Y., Visible light photocatalytic activity of Cu, N co-doped carbon dots/Ag_3PO_4 nanocomposites for neutral red under green LED radiation, Colloid Surf. A, 578, 123643 (1-8), 2019.

[25] Tijani J. O., Momoh U. O., Salau R. B., Bankole M. T., Abdulkareem A. S., Roos W. D., Synthesis and characterization of Ag_2O/B_2O_3/TiO_2 ternary nanocomposites for photocatalytic mineralization of local dyeing wastewater under artificial and natural sunlight irradiation, Environ. Sci. Pollut. Res., 26 (19), 19942-19967, 2019.

[26] Duran-Alvarez J. C., Santiago A. L., Ramirez-Ortega D., Acevedo-Pena P., Castillon F., Ramirez-Zamora R. M., Zanella R., Surface modification of B-TiO_2 by deposition of Au nanoparticles to increase its photocatalytic activity under simulated sunlight irradiation, J. Sol-Gel Sci. Technol., 88 (2), 474-487, 2018.

[27] Surowka M., Kobielusz M., Trochowski M., Buchalska M., Kruczala K., Bros P., Macyk W., Iron and other metal species as phase-composition controllers influencing the photocatalytic activity of TiO_2 materials, Appl. Catal., B, 247, 173-181, 2019.

[28] Chowdhury S., Jiang Y., Muthukaruppan S., Balasubramanian R., Effect of boron doping level on the photocatalytic activity of graphene aerogels, Carbon, 128, 237-248, 2018.

[29] Brooms T. J., Otieno B., Onyango M. S., Ochieng, A., Photocatalytic degradation of P-Cresol using TiO_2/ZnO hybrid surface capped with polyaniline, J. Environ. Sci. Health Part A-Toxic/Hazard. Subst. Environ. Eng., 53 (2), 99-107, 2018.